A Multilevel Approach for Optimal Participating of Wind Farms at Reactive Power Balancing in Transmission Power System

Amir Ahmidi, *Member, IEEE,* Xavier Guillaud, *Member, IEEE,*
Yvon Besanger, *Senior Member, IEEE,* and Régis Blanc

Abstract—According to the different grid codes, wind farms which are connected to transmission network have to supply not only the active power, but also the reactive power to the grid. The aim of the proposed work is to present an optimal multilevel control system which allows the doubly fed synchronous generator based wind farms to participate at reactive power balancing in transmission network. In this method, we use a multilevel control system, consisting of two levels to regularly calculate the references of all wind turbines. First, the algorithm calculates the optimal reference values of reactive power for each wind farm at its point of common coupling with the grid. Second, it calculates the references of the wind turbines in each wind farm to consider the optimal reactive power references obtained at the first level. The proposed multilevel control system recalculates the available reserve of the reactive power to determine the optimal references. A probabilistic method based on auto regressive integrated moving average is used to predict the available reactive power reserve which is strongly related to uncertain nature of wind speed. This control system is developed particularly to control the wind farm reactive power injected into the grid. It is well adapted to fluctuating nature of the wind speed. It is also faster than other methods with a global single level optimal control system.

Index Terms—Optimal multilevel control system, transmission power system, voltage/var control, wind farm reactive power forecasting.

I. INTRODUCTION

IN RECENT YEARS, the integration of wind generations into the power grid has grown significantly. Most wind farms are connected to the distribution level, which limits the nominal power capacity of wind farm. For example, in France, the wind farm production is limited to 12 MW at the

distribution level. However, in some areas, the wind generation potential is very important, which would permit building the wind farms with a power capacity as large as several hundred megawatts. This range of power capacity requires a direct connection to the transmission network. These wind farms have to fulfill the same requirements as the existing large conventional power plants. These requirements are defined in the grid codes which can be modified individually by the grid utility. Depending on the structure of the grid, transmission system operators (TSO) change the limits of desired reactive power generation/absorption for different voltages [1]–[5].

The principal objective of this paper is to give an optimal response, as a wind farm producer, to a reactive power demand by TSO. For this purpose, first we need to define the reactive power capability of the wind farms, which depends mainly on the capability of the wind turbines. The PQ diagrams of different types of the wind turbine are discussed in different references. Reference [6] explored the different combinations of rotor's and grid side converters' reactive power control. It also illustrated the PQ-diagram of a doubly fed synchronous generator (DFIG) connected to an infinite bus for different terminal voltages. References [7] and [10] presented a steady-state PQ-diagram for a variable speed wind turbine equipped with a DFIG. They also presented the limitations in reactive power production, caused by current and voltage of both the rotor and the stator. Reference [8] provided a detailed mathematical model of a DFIG, expressed in its stator-flux-oriented reference frame in a state-equation form.

In this paper, we first recall the steady-state PQ-diagram of a single wind turbine equipped with a DFIG. We will adapt this diagram for a 2 MW wind turbine which is used in our study case [9].

In the second step, we define the wind farm's reactive power capability. In the literature, [11] and [15] provided an overview about the available options to supply reactive power by wind farms to the power grid. They explained also the reactive power generation capability of DFIG wind turbines during very low voltage periods. References [12] and [13] studied the influence of large scale wind farm connected to power distribution system. Reference [14] developed a complete model of a wind farm using DFIG. It also studied the performance of the model for active/reactive power regulation.
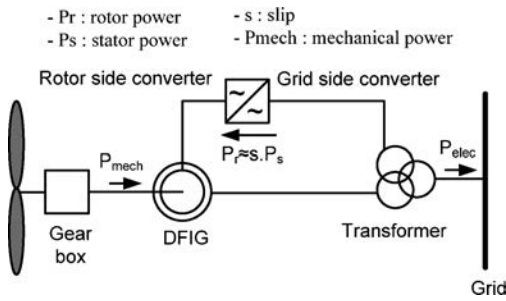
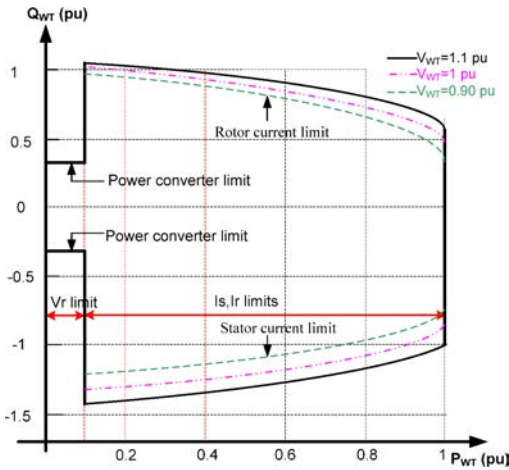Fig. 1. DFIG wind turbine power grid connection.

Fig. 2. DFIG wind turbine PQ-diagram.

In this paper, we propose a method to calculate the reactive power capability of a wind farm which includes the participation of the cables and the transformers 0.69/20 kV inside the farm. It is also limited by the constraints on voltage deviation for the buses inside the wind farm. In order to take into account the differences of power production between wind turbines in the same farm, we use a probabilistic method based on a Monte Carlo algorithm [24].

In the third step, we need an optimization algorithm which can coordinate the reactive power production of all wind turbines. The different methods for power grid control based on multiobjective functions are discussed in different references. Reference [16] proposed a particle swarm optimization algorithm for economic power dispatch in the presence of the wind power generation. References [17] and [21] explained a voltage control method based on a generic algorithm. This algorithm coordinates the distributed installations, such as the load ratio control transformer, step voltage regulator, and wind turbines. References [18]–[20] proposed a coordinated voltage control based on multiobjective algorithm. It improves the use of distributed generations to maintain the voltage at its set-point value for the specific nodes called pilot buses. In this paper, we propose a multilevel control system to calculate the optimal reactive power references for all the wind turbines, while considering all voltage and reactive power capability limits. Since the reactive power capability depends on the active power delivered by the wind turbine, we use a probabilistic method based on auto regressive integrated

moving average (ARIMA) method to forecast the wind farm production at each control system action sample time [22], [23].

In addition, we have to consider that these wind turbines are connected to the transmission network within an OLTC transformer. The optimization process coordinates the reactive power of the wind farms and the control OLTC.

We will apply this optimization method to a group of three wind farms with a total active power of 50 MW. The PCCs substations of all the wind farms are connected to a 20 kV bus.

The results show that the proposed multilevel approach can be an effective and fast way for the wind farm reactive power participation in transmission power system.

II. WIND FARM REACTIVE POWER CAPABILITY

The first step is to present the PQ-diagram of a DFIG wind turbine.

A. PQ-Diagram of a DFIG Wind Turbine

The connection of a DFIG wind turbine to power grid is shown in Fig. 1. A steady-state diagram of the reactive power capability of a DFIG wind turbine is presented in [7] and [13].

The power converter presented in Fig. 1 is used to transmit rotor power to support maximum power production.

Practically, we should use an oversized converter in order to provide also the reactive power even if the generator maximum active power is provided (usually a 30% oversized converter is used). This participation is limited by the stator current (I_s), the rotor current (I_r), the rotor voltage (V_r) and it will be also related to the slip. The stator current limit depends on DFIG design; the limits of rotor voltage and current depend on DFIG and also on the power converter design. These constraints are summarized in the wind turbine PQ-diagram which is presented in Fig. 2.

We find that, for a production smaller than 0.1 pu, the rotor voltage will limit the reactive power production. In this condition, using the reactive power reserve of DFIG generator is not recommended.

Consequently, we use only the converter to provide the reactive power. Therefore, the PQ-diagram will have a discontinuity while passing from alone converter reactive power reserve to entire converter and generator reactive power reserve.

B. PQ-Diagram of a DFIG Wind Farm

The transformers and the cables have a significant role in the reactive power capability of a wind farm. The PQ-diagram of an actual wind farm which is situated in the North of France is presented in Fig. 3. This wind farm is composed of five DFIG 2 MW wind turbines.

These curves are presented for different operating voltage values at the wind farm PCC. The variation of the operating voltage at wind farm PCC is ±5% of its contractual voltage. For this wind farm, the contractual voltage is set to 1.05 pu of the PCC nominal voltage ($V_{PCCnominal} = 20$ kV). That is why the operating voltage at PCC is considered between 1 and 1.1 pu.
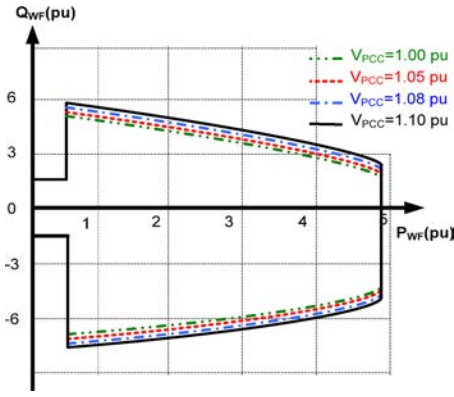
Fig. 3.   DFIG wind farm PQ-diagram.

Fig. 4.   DFIG wind farm PQ-diagram considering the buses voltage constraint.

We calculate the maximum reactive power capability at the PCC for different voltage values at PCC and different production values of wind turbines. Fig. 3 shows the results considering that the power productions of all the wind turbines in the wind farm are the same ($V_{base} = 20 \, kV$, $S_{base} = 2 \, MVA$).

The asymmetry in the diagram is due to the absorption of a significant reactive power by transformers during an important production of the wind farm.

We must also take into account the maximum voltage constraint at all the wind turbine buses inside the wind farm. The maximum voltage variation at the DFIG wind turbine terminals considered here is 10% of its nominal voltage.

An algorithm based on load flow equations and sensitivity matrixes is used to satisfy the constraint [26], [27]. Equations (1) and (2) calculate the maximum reactive power production/absorption of each wind turbine for the maximum voltage deviation at its bus.

For the upper limit

$$Q_{WT\,const\,2}^{max} = (V_{WT}^{max} - V_{WT}) * S_{V_g Q_g} + Q_{WT}. \tag{1}$$

For the lower limit

$$Q_{WT\,const\,2}^{min} = (V_{WT}^{min} - V_{WT}) * S_{VgQg} + Q_{WT}. \tag{2}$$

V_{WT}^{max} and V_{WT}^{min} are, respectively, the maximum and minimum voltage deviation for a wind turbine.

V_{WT} and Q_{WT} are, respectively, the voltage and the active power calculated by the load flow program at wind turbine terminals for each operating point of the wind farm.

$S_{V_g Q_g}$ is the sensitivity matrix, representing the relation between voltage and reactive power variations at wind turbines buses.

Considering all these constraints, (3) and (4) show that the reactive power production/absorption margins of each wind turbine are defined with the most restrictive constraint between them.

For the upper limit

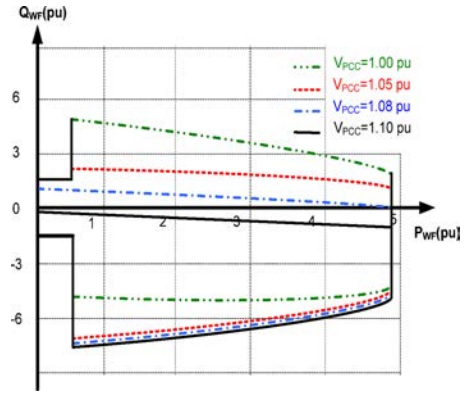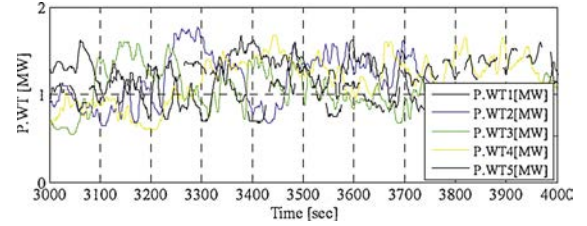$$Q_{WT}^{max} = min(Q_{WT\,const\,1}^{max}, Q_{WT\,const\,2}^{max}). \tag{3}$$

Fig. 5.   Experimental data measurements.

For the lower limit

$$Q_{WT}^{min} = max(Q_{WT\,const\,1}^{min}, Q_{WT\,const\,2}^{min}). \tag{4}$$

$Q_{WT\,const\,1}^{max}$ and $Q_{WT\,const\,1}^{min}$ are the maximum reactive power production/absorption by considering the wind turbine PQ-diagram presented in Fig. 2.

$Q_{WT\,const\,2}^{max}$ and $Q_{WT\,const\,2}^{min}$ are the maximum reactive power production/absorption by considering (1) and (2).

Finally, the proposed algorithm finds the limits of the wind farm by integrating the participation of transformers and cables. The reactive power reserve of the wind farm is the total of wind turbines reactive reserves in the wind farm excluding the reactive power losses in the transformers and the cables. The active power production of the wind farm is calculated using the same method.

The results for different voltage values of PCC and different production values of wind turbines are shown in Fig. 4.

We realized that as long as the voltage of the PCC is under 1 pu, the PQ-diagram margins (green curve) are only defined by the limits of reactive power production. However, as the PCC voltage increases, the PQ diagram margins (blue curve) are limited by the maximum bus voltages of the wind farm. ($V_{base} = 20 \, kV$, $S_{base} = 2 \, MVA$).

C. Influence of the Wind Turbines Unpredicted Productions

The calculation of wind farm PQ-diagrams is based on the same power productions assumption for all the wind turbines in the wind farm. However, experimental data measurements in Fig. 5 show that the hypothesis is not valid. The power production of wind turbines is different even if they are located in the same neighborhood.

TABLE I
CORRELATION MATRIX BETWEEN ACTIVE PRODUCTIONS
OF WIND TURBINES

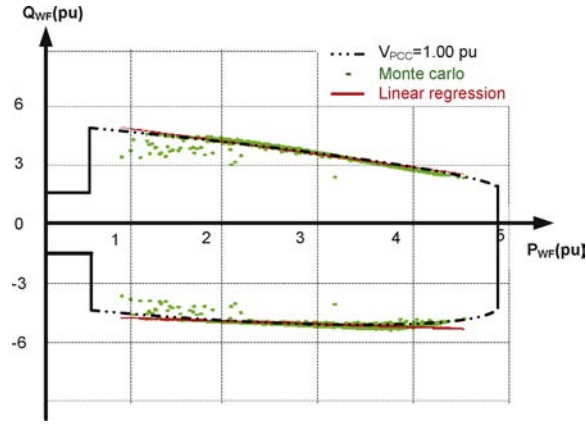| Correlation Matrix					
	$WT1$	$WT2$	$WT3$	$WT4$	$WT5$
$WT1$	1.0000	0.5096	0.7074	0.6600	0.5599
$WT2$	0.5096	1.0000	0.5893	0.6491	0.3123
$WT3$	0.7074	0.5893	1.0000	0.7622	0.5121
$WT4$	0.6600	0.6491	0.7622	1.0000	0.5132
$WT5$	0.5599	0.3123	0.5121	0.5132	1.0000

Fig. 6. DFIG wind farm PQ-diagram for $V_{PCC} = 1$ pu (Monte Carlo algorithm for 1000 tries) (MAPE = 2.8%).
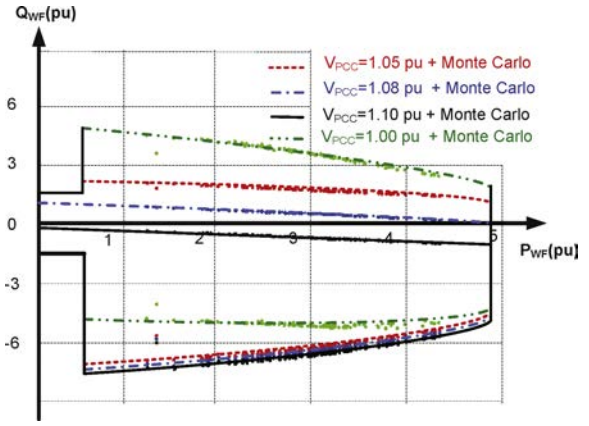

Fig. 7. DFIG wind farm PQ-diagram for different PCC voltages (Monte Carlo algorithm for 100 tries).

Fig. 8. Wind farm power production forecasting algorithm.

For this purpose, we have to find the real correlation factors between the wind turbines productions. This correlation matrix is presented in Table I and is based on a 2 h sample period of production measurements. The results show that the correlation factors vary between 0.3123 and 0.7622.

We also integrate the Monte Carlo method in the algorithm, because we need a random process for wind power production to calculate the real PQ-diagram of the wind farm.

Using the Monte Carlo method, we model the active production of each wind turbine by a normal distribution. Indeed, in statistic processing, any random value follows a normal distribution using a sufficient large sample size [24].

By considering the correlation matrix presented in Table I and for a large number of random wind turbines active productions, the algorithm described in Section II-B recalculates the PQ-diagram of the wind farm. This strategy gives us a cloud of points which is shown in Fig. 6. We use a linear regression on the cloud of points to estimate the PQ-diagram. The mean absolute percentage error (MAPE) indicates also the accuracy degree of the estimated diagram. One thousand tries of the Monte Carlo method show a high similarity between the PQ-diagram obtained using a correlation unit matrix and the PQ-diagram using the real correlation matrix between the wind turbines productions. The MAPE for this case is 2.8%.

Once the accuracy of Monte Carlo method is proven, it is used to calculate the different curves for different voltage values of PCC and different production values of the wind turbines. The results presented in Fig. 7 show a perfect similarity between PQ-diagrams obtained using a correlation unit matrix and PQ-diagrams using the real correlation matrix between the wind turbines productions.

D. Provision of Wind Farm Active Power Production

In Section III, we show that the proposed multilevel control system needs available reactive power reserve of wind farms to operate. The PQ-diagram of the wind farm presented in Fig. 7 shows that, at each instant, the reserve depends on
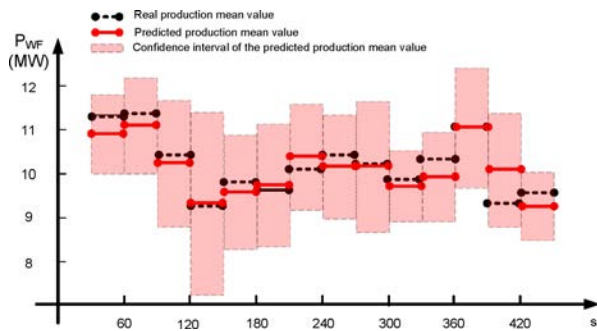
Fig. 9. Wind farm power production forecasting.

Fig. 10. Wind farms connection.

the active power delivered by the wind turbine. It means that the available reactive power reserve fluctuates as like as the wind active power production. Therefore, a good prediction of active power production and reactive power reserve of wind farms is necessary at each control system action sample time. We consider that the control system acts with sample time T_{int} (= 30 s), and t_n is the instant of the nth control system action. Therefore, a good estimation of the average active production between $[t_n \ t_n + T_{int}]$ based on the active power data between $[t_n \ t_n - T_{int}]$ permits an optimal accomplishment of the varying reactive capability of the wind farm. Among many methods which could be used to solve the problem, we choose a general class of model known as ARIMA model [22], [23]. This method is implemented in "R" statistical software [25] which is integrated in MATLAB Simulink. The general representation of the estimation algorithm of power production is shown in Fig. 8.

For a measurement period of 450 s, we compare the forecasted production mean value using the real production mean value for the time intervals of T_{int} (=30 s). The results in Fig. 9 show that the real production mean value is always included in the confidence interval of the predicted production mean value. This indicates a very good estimation of the wind farm power production by the ARIMA method.

Once the wind farm reactive power capability is identified, we can develop the multilevel control system for optimal participating of the wind turbines to balance the reactive power of the transmission system.

III. MULTILEVEL CONTROL SYSTEM

Fig. 10 presents a group of three wind farms, 16 MW, 16 MW, and 18 MW connected to a 20 kV/63 kV OLTC using 5, 7, and 10.5 km cables. We want to deliver a reactive power to the HV network (Q_{TSO}^{ref}). This reactive power is imposed by the TSO. A multilevel control system is proposed to coordinate the reactive power references for each of the wind farms and the OLTC control. The fluctuating nature of wind requires a control system that can react quickly to adapt the power references in respect with the wind variation. But, a global optimization algorithm which calculates the reactive power reference for many wind turbines and OLTC is very time-consuming. Therefore, we propose a two-level control system: the first level control defines the reactive power
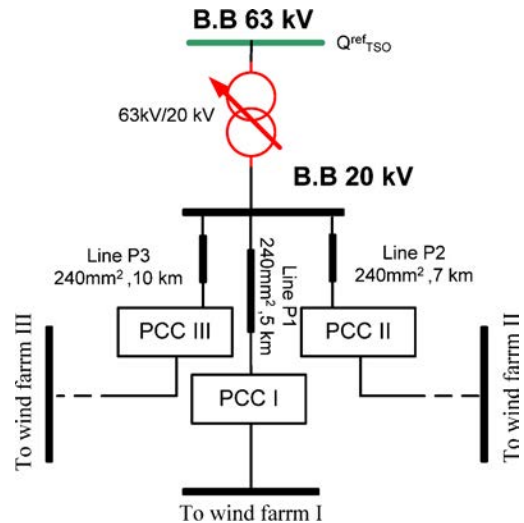
reference for each wind farm and OLTC. The second level control defines the reactive power reference for each wind turbine.

A. First Level

The first level uses a multiobjective optimization function and a global controller to calculate the reactive power references of each wind farm at their corresponding PCC and the reference voltage of OLTC transformer. This objective function is detailed below.

1) *Minimization of Power Losses Inside of Wind Farms:* The primary objective of this function is to minimize losses in the interconnection cables between the PCCs of each wind farm and the OLTC transformer of 63/20 kV. For this purpose, the load flow equations are used

$$\text{Minimize} \quad A_p \cdot \sum_{\text{Cables}} Re(\Delta V_i \cdot I_i^*) \tag{5}$$

where ΔV_i is cable terminals voltage variation i, I_i is cable current i, and A_p is the weighting factor for active power losses.

2) *Minimization of OLTC Operation:* To reduce the OLTC operation number, another objective is added. It minimizes the difference between the OLTC transformer voltage (V_T) before the optimization and the corresponding OLTC reference voltage values (V_T^{ref})

$$\text{Minimize} \quad \left| V_T^{ref} - V_T \right|. \tag{6}$$

3) *Constraint for the Control of the Reactive Power at the Grid Connection Point:* The initial and main objective of the control system is to control the reactive power at the grid connection point. This means an equality between the measured reactive power ($Q_{B.B.63}^{mes}$) at the wind farms grid connection point and the reference value applied by the TSO (Q_{TSO}^{ref}). We introduce this objective as an equality constraint

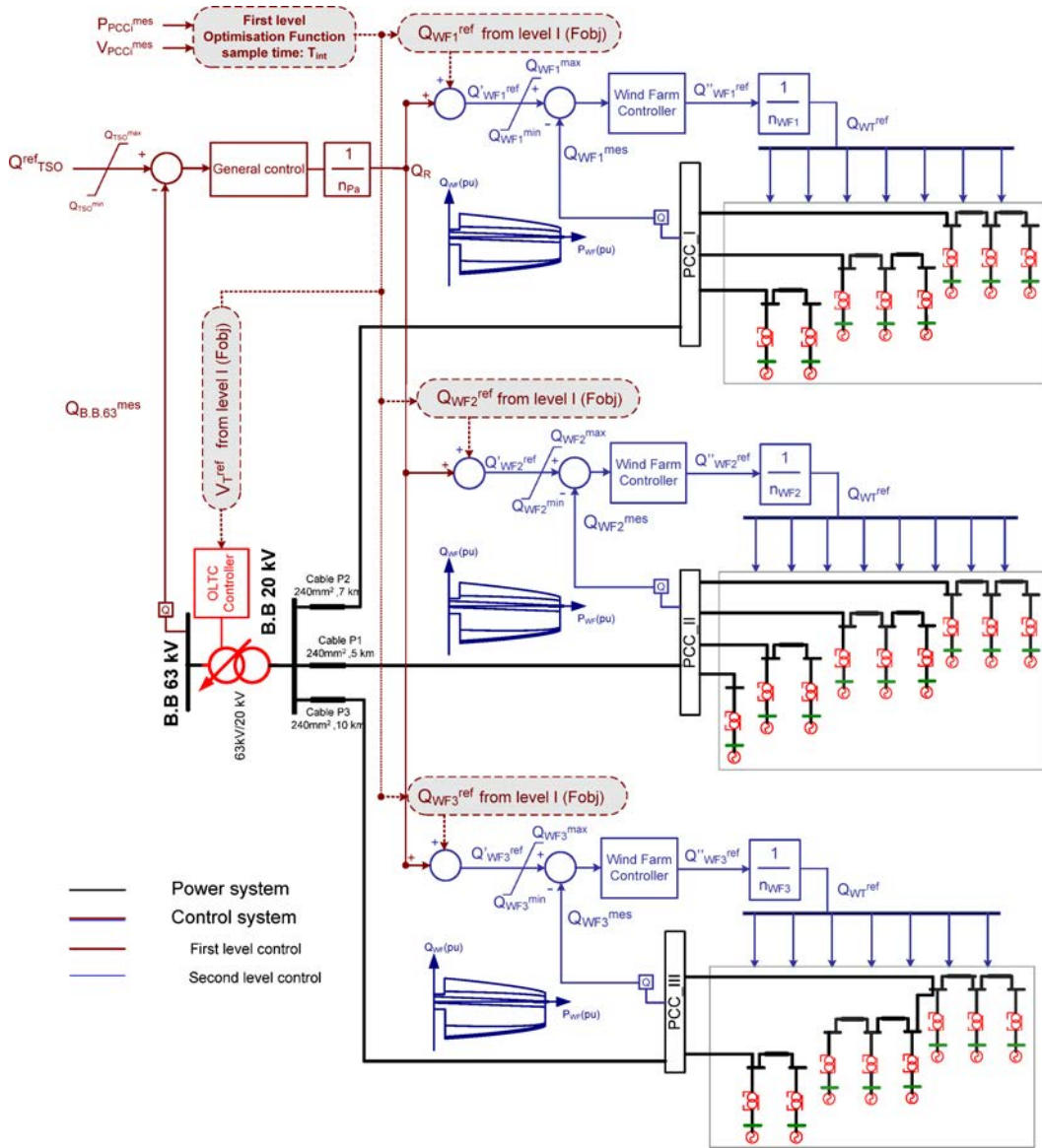$$Q_{TSO}^{ref} = Q_{B.B.63}^{mes}. \tag{7}$$

Fig. 11.   Multilevel control system.

4) *Functional and Contractual Constraints Satisfaction:*
We also have to comply with the reactive power limits defined
in Sections II-B and II-C at all PCC buses.

We have introduced this objective as an inequality constraint

$$Q_{WF_i}^{\min} < Q_{WF_i}^{\text{ref}} < Q_{WF_i}^{\max} \quad i = I, II, III. \tag{8}$$

$Q_{WF_i}^{\max}$ and $Q_{WF_i}^{\min}$ are calculated for each wind farm considering
the PQ-diagram presented in Fig. 4. So, the optimization
function includes two objectives presented in (9)

$$F_{\text{obj}}(Q_{WF\,i}^{\text{ref}}, V_T^{\text{ref}}) = A_P.n_P \sum_{\text{Cables}} Re(\Delta V_i \cdot I_i^*) \\ + A_{V_T} \cdot n_{V_T} \left| V_T^{\text{ref}} - V_T \right|. \tag{9}$$

n_P, n_{v_T} are normalization factors, A_p, A_{V_T} are weighting
factors

5) *Global Controller:* As shown in Fig. 11, a controller
located at the connection point of the transmission network
guaranties a good adjustment of the control system response to

the TSO reactive power reference. It compensates the residual
error between $Q_{\text{TSO}}^{\text{ref}}$ and $Q_{B.B.63}^{\text{mes}}$ by using a PI controller. The
output of the controller (Q_R) is distributed between all wind
farms identically to correct $Q_{WF\,i}^{\text{ref}}$ slightly. The actual reactive
power reference is named $Q_{WF\,i}^{'\text{ref}}$.

B. Second Level

The second level of the control system is based on a closed
loop controller (wind farm controller) to generate the reactive
power reference for each wind turbine ($Q_{\text{WT}}^{\text{ref}}$) considering the
wind farm reactive power reference. The controller generates
a third reactive power reference $Q_{WF\,i}^{''\text{ref}}$ which is distributed
identically between each wind turbine (see Fig. 11).

IV. CASE STUDY

We assess the performance of the proposed multilevel
control system on the set of three wind farms presented in
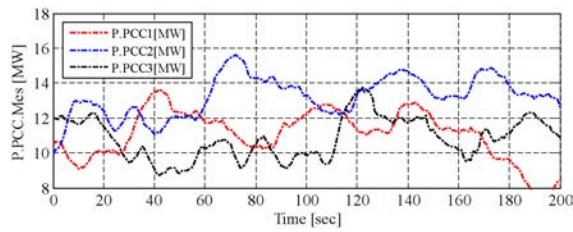Fig. 10.

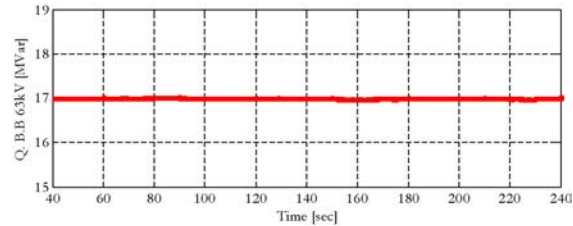Fig. 12.   Wind farms PCCs active power production measurements.

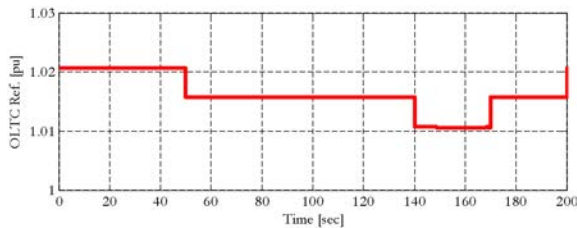Fig. 13.   Reactive power profile of 63 kV transmission bus.

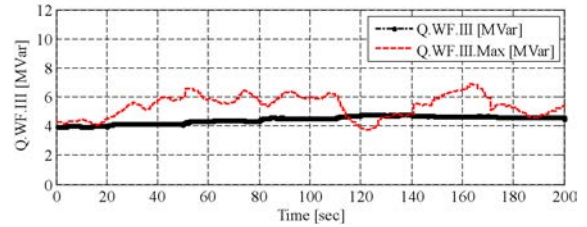Fig. 14.   OLTC reference voltage.

Fig. 15.   Reactive power reference and variation of reactive power capability for the three wind farms.

Fig. 16.   OLTC reference voltage.

Fig. 12 presents the variation of active power production at wind farms PCCs caused by a wind speed variation for a period of 200 s. We want to verify the performance of the proposed multilevel control system for this production period while a reactive power production reference of 17 MVAR is requested by the TSO.

We select a wind power profile that is able to represent a large difference of power production between the different wind farms.

First, we present some simulation results while minimizing the power losses. The present simulation results are obtained for a 1 pu on the 63 kV bus voltage. Fig. 13 proves that the reactive power on this bus is well controlled.

Fig. 14 shows that the OLTC reference is as high as possible when minimizing the losses. Consequently, as shown in Fig. 15 the limits in reactive are low and the references for each wind farm reach the limits.

We have modeled the discrete action of the OLTC by quantifying its reference voltage. We have chosen 21 steps on the whole range of operation. We notice frequent steps in Fig. 15 for the OLTC voltage reference. Clearly, this is not acceptable for the OLTC because it decreases its lifetime and increases the maintenance costs. The measured losses during the 270 s of simulation are 58.5 kWh.

In a second simulation, we choose to minimize the OLTC operations. Fig. 16 shows that with the chosen quantification, no change is noticed on OLTC voltage reference.
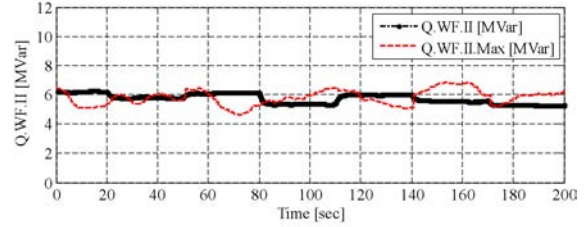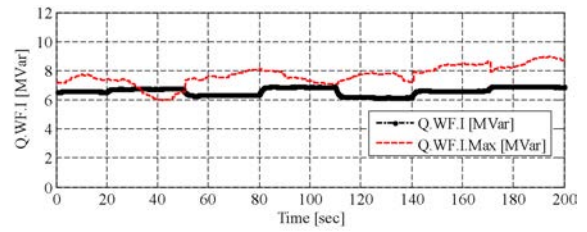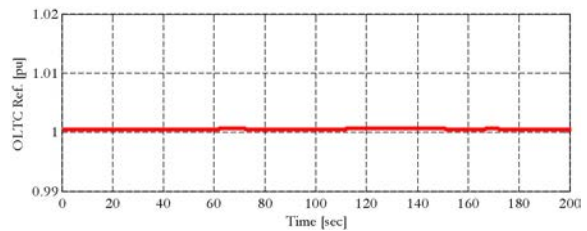
All the reactive power references are within the dynamic reactive power limit calculated by the algorithm. The measured losses during the 270 s of simulation are 60.2 kWh which shows a slight increasing of 3% for the losses. The algorithm splits the reference of reactive power in three for each wind farm. We find that the farms I and II contribute more to the reactive power production compared to the farm III because their electrical distance to the OLTC is smaller. The difference is due to the usage of the optimization function to reduce the power losses.

Fig. 18 shows voltages of the wind turbine buses inside the wind farm I. We find that the reactive power references calculated by the first level meet also the voltage constraints on these buses. This is due to the characterization of the wind farms PQ-diagrams presented in Section II-B. The voltages of wind turbine buses inside the wind farms II and III are not shown but the voltage constraints are also met for these wind farms.

Fig. 19 illustrates the reactive power capability variation of one of the wind turbines in the wind farm I. We can verify that the reactive power reference is always inside admissible margins. The reactive power for each wind turbine has been
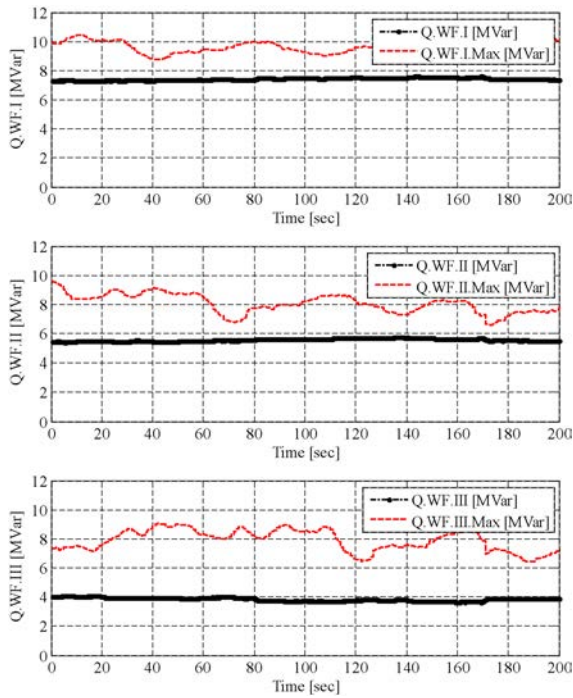
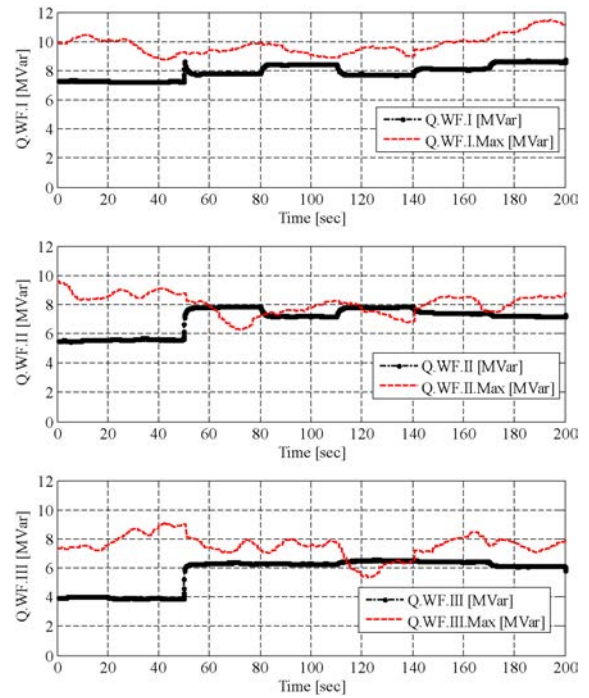Fig. 17.   Variation of reactive power reference and reactive power capability for the three wind farms.
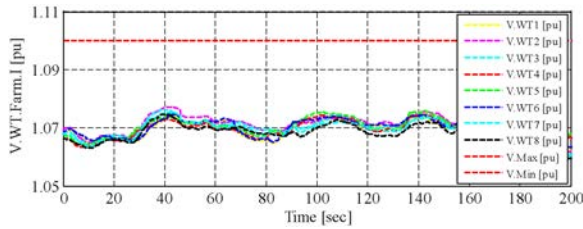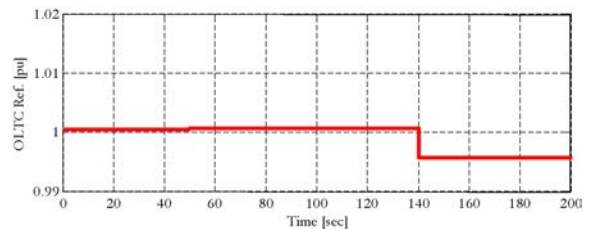

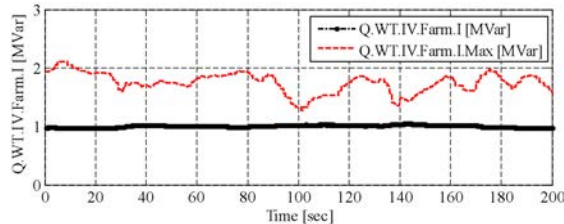Fig. 18.   Wind turbines buses voltages.

Fig. 19.   Variation of reactive power capability of wind turbines.

analyzed and found within the limits of the reactive power capability.

Figs. 20 and 21 show the behavior of the system with a steep increase of reactive power reference from 17 MVAR to 22 MVAR at $t = 50$ s. The reactive reference is increased for all the wind turbines. The wind turbines 2 and 3 are close to their limits. Exceeding the limits, the OLTC starts to decrease the voltage ($t = 140$ s) and increase the reactive power capability.

V. CONCLUSION

In this paper, we proposed a multilevel approach for optimal participation in reactive power balancing of wind farms connected to the transmission grid. For this purpose, we defined

Fig. 20.   Variation of reactive power reference and reactive power capability for the three wind farms.

Fig. 21.   OLTC reference voltage.

reactive power capability of a DFIG wind turbine. Afterwards, we proposed a method to find the reactive power capability of a wind farm by considering the effect of all the cables, 0.69/20 kV transformers inside the farm and the constraints on voltage deviation of the buses inside the wind farm.

In order to have a more practical wind farm PQ-diagram, we used a probabilistic method based on Monte Carlo algorithm to consider the difference of power production between the wind turbines of a same farm.

In order to find the available reactive power reserve of wind farms which fluctuates as like as the wind active power production, we used a probabilistic method based on ARIMA. It permits us to forecast the reactive power reserve of wind farms at each control system action sample time.

We proposed an optimal multilevel control system consisting of two levels to calculate the reactive power references of all the wind turbines. Considering the physical well-known constraints, we had to minimize the OLTC operations. So we chose a set of parameters where the OLTC does not change too much.

We applied this optimization method to a group of three wind farms. The results show that the proposed multilevel approach is an effective and fast method regarding our objectives.

In further works, we will implement this method on a real time digital simulator before the implementation on a real site. This step is particularly interesting because it allows not only the evaluation of the control system in real time, but also the setup of the physical communication system.

APPENDIX A
CABLES PARAMETERS

Connection From To	Section	R (Ω/km)	L (mH/km)	C μF/km
WT–PCC	240 Al	0.16	0.33	0.36
PCC–B.B.63 kV	240 Cu	0.088	0.316	0.365

APPENDIX B
DFIG PARAMETERS

Symbol	Quantity	Unit	Value
P_n	Nominal active power	MW	2
V_{sn}	Nominal stator voltage	V	1650
V_{rn}	Rotor voltage with blocked rotor	V	690
n_{winding}	Turn ration between rotor and stator		2.43
R_s	Stator resistance	Ω	0.00206
X_s	Stator leakage resistance	Ω	0.032
X_m	Main resistance	Ω	0.83
R_r	Rotor resistance (referred to stator side)	Ω	0.0028
X_r	Rotor leakage resistance (referred to stator side)	Ω	0.021
V_A	Start speed	m/s	3.5
V_C	Nominal speed	m/s	13
V_D	Cutting speed	m/s	25
Spc	Converter's apparent power	MVa	0.6

APPENDIX C
0.69/20 KV TRANSFORMER PARAMETERS

Symbol	Quantity	Unit	Value
P_n	Nominal active power	MW	2.3
V_{pn}	Nominal primary voltage	kV	20
V_{sn}	Nominal secondary voltage	kV	0.69
X/R	Transformer X/R ratio	–	10
$U_{CC}\%$	Short circuit impedance	–	7.85

APPENDIX D
20/63 KV OLTC TRANSFORMER PARAMETERS

Symbol	Quantity	Unit	Value
P_n	Nominal active power	MW	50
V_{pn}	Nominal primary voltage	kV	63
V_{sn}	Nominal secondary voltage	kV	20
X/R	Transformer X/R ratio	–	6
$U_{CC}\%$	Short circuit impedance	–	12

REFERENCES

[1] E.on Netz. (2006). *Grid Code, High and Extra High Voltage* [Online]. Available: http://www.eon-etz.com
[2] National Grid Electricity Transmission plc. (2009). *The Grid Code* [Online]. Available: http://www.nationalgrid.com
[3] Electricité de France. (2006). *Relatif aux prescriptions techniques de conception et de fonctionnement pour le raccordement d'une installation de production d'énergie électrique au réseau public HTB=50 KV des Zones non interconnectées* [Online in French]. Available: http://sei.edf.com
[4] ESB National Grid. (2007). *Grid Code* [Online]. Available: http://www.esb.ie
[5] I. Erlich and U. Bachmann, "Grid code requirements concerning connection and operation of wind turbines in Germany," in *Proc. IEEE Power Eng. Soc. General Meeting*, vol. 2. Jun. 2005, pp. 1253–1257.
[6] M. Kayikci and J. V. Milanovic, "Reactive power control strategies for DFIG-based plants," *IEEE Trans. Energy Convers.*, vol. 22, no. 2, pp. 389–396, Jun. 2007.
[7] T. Lund, P. Soerensen, and J. Eek, "Reactive power capability of a wind turbine with doubly fed induction generator," *Wind Energy J. Wiley*, vol. 10, no. 4, pp. 379–394, 2007.
[8] G. Tapia, A. Tapia, and J. X. Ostolaza, "Two alternative modeling approaches for the evaluation of wind farm active and reactive power performances," *IEEE Trans. Energy Convers.*, vol. 21, no. 4, pp. 909–920, Dec. 2006.
[9] REpower Systems, *Electrical Description REpower 2M (Elektrische Beschreibung REpower 2M), in German*, REpower Systems, Rendsburg, Germany, 2006.
[10] A. Petersson, "Analysis, modeling and control of doubly-fed induction generators for wind turbines," Ph.D. dissertation, Dept. Elect. Eng., Chalmers Univ. Technol., Gothenburg, Sweden, 2005.
[11] I. Erlich, M. Wilch, and C. Felte, "Reactive power generation by DFIG based wind farms with AC grid connection," in *Proc. Eur. Conf. Power Electron. Applicat.*, Sep. 2007, pp. 1–10.
[12] V. Akhmatov, "Analysis of dynamic behavior of electric power systems with large amount of wind power," Ph.D. dissertation, Dept. Elect. Eng., Tech. Univ. Denmark, Lyngby, Denmark, 2003.
[13] T. Lund, "Analysis of distribution systems with a high penetration of distributed generation," Ph.D. dissertation of Electrical Power Engineering, Tech. Univ. Denmark, Lyngby, Denmark, 2007.
[14] A. Tapia, G. Tapia, and J. X. Ostolaza, "Reactive power control of a wind farm for voltage control applications," *Renewable Energy J. Elsevier*, vol. 29, no. 3, pp. 377–392, Mar. 2004.
[15] I. Erlich, W. Winter, and A. Dittrich, "Advanced grid requirements for the integration of wind turbines into the German transmission system," in *Proc. IEEE Power Eng. Soc. General Meeting*, Jun. 2006, p. 7.
[16] L. F. Wang and C. Singh, "Balancing risk and cost in fuzzy economic dispatch including wind power penetration based on particle swarm optimization," *Electr. Power Syst. Res. Elsevier*, vol. 29, no. 8, pp. 1361–1368, 2008.
[17] T. Senjyu, Y. Miyazato, A. Yona, N. Urasaki, and T. Funabashi, "Optimal distribution voltage control and coordination with distributed generation," *IEEE Trans. Power Deliv.*, vol. 23, no. 2, pp. 1236–1242, Apr. 2008.

[18] A. Ahmidi, X. Guillaud, Y. Besanger, and R. Blanc, "Wind generations participation at optimal voltage regulation in distribution networks," in *Proc. CIGRÉ Canada Conf. Power Syst.*, Oct. 2009, pp. 1–9.

[19] J. P. Paul, J. Y. Léost, and J. M. Tesseron, "Survey of the secondary voltage control in France: Present realization and investigation," *IEEE Trans. Power Syst.*, vol. 2, no. 2, pp. 505–511, May 1987.

[20] O. Richardot, A. Viciu, Y. Besanger, N. Hadjsaid, and C. Kieny, "Coordinated voltage control in distribution networks using distributed generation," in *Proc. IEEE PES Conf. Transmission Distribution*, May 2006, pp. 1196–1201.

[21] H. M. Ma, K. F. Man, and D. J. Hill, "Control strategy for multiobjective coordinate voltage control using hierarchical genetic algorithms," in *Proc. IEEE Int. Conf. Ind. Technol.*, Dec. 2005, pp. 158–163.

[22] R. H. Shumway and D. S. Stoffer, *Time Series Analysis and Its Applications with R Examples*. New York: Springer, 2010.

[23] P. Chen Pedersen, T. Bak-Jensen, and B. Zhe Chen, "ARIMA-based time series model of stochastic wind power generation," *IEEE Trans. Power Syst.*, vol. 25, no. 2, pp. 667–676, May 2010.

[24] A. Papoulis, *Probability, Random Variables, and Stochastic Processes*. New York: McGraw-Hill, 1965.

[25] R. A. Muenchen and J. M. Hilbe, *R for Stata Users*. New York: Springer, 2010.

[26] J. Momoh, *Electric Power System Application of Optimization*. New York: Dekker, 2001.

[27] P. S. Kundur, *Power System Stability and Control*. New York: McGraw-Hill, 1993.

Amir Ahmidi (M'09) received the M.Sc. degree from the National Polytechnic Institute of Grenoble, Grenoble, France, in 2007. He is currently pursuing the Ph.D. degree in wind farm participation in ancillary services with the University of Lille-Nord de France, Ecole Centrale de Lille, Villeneuve d'Ascq Cedex, France. His thesis is carried out in cooperation with the Maia Eolis Company, Lille, France, the Laboratory of Electrical Engineering and Power Electronic of Lille, Lille, and the Grenoble Electrical Engineering Laboratory, Grenoble. His thesis is a part of research and development projects of the Maia Eolis Company which is a wind farm developer in the North of France.

Xavier Guillaud (M'02) received the Ph.D. degree in electrical engineering from the University of Science and Technology of Lille, Lille, France, in 1992.

He joined the Laboratory of Electrical Engineering and Power Electronics, Lille, in 1993. Currently, he is a Professor with the University of Lille-Nord de France, Ecole Centrale de Lille, Villeneuve-d'Ascq Cedex, France. Since 2001, he has worked on the integration of distributed generation systems in electrical grids and smartgrids. His main topics of interest concern the modeling and the control of power electronics systems.

Yvon Besanger (SM'06) received the Ph.D. degree in electrical engineering from the Grenoble Institute of Technology, Grenoble, France, in 1996.

He is currently a Professor with the Engineering School for Energy, Water and Environmental Sciences, Grenoble, and the Grenoble Electrical Engineering Laboratory, Saint Martin d'Hères Cedex, France. His current research interests include power system security, distribution networks operation, and reliability and smartgrids.

Régis Blanc received the Electrical Engineering Diploma from the École Nationale Supérieure des Mines de St-Etienne, St-Etienne, France, in 1988.

He is currently the Chair of the Research and Development Department, Maia Eolis Company, Lille, France, where he works on different subjects of wind farm supervision and control, wind power forecasting, and wind farm participation in ancillary services.